EUROPEAN ORGANIZATION FOR NUCLEAR RESEARCH

DIRAC note 2023-01

DIRAC/PS212

CERN-EP-2023-XXX
23 July 2023

The investigation of the Coulomb interaction in $\pi^+\pi^-$ pair production and application of the effect to the event simulation and setup description

A. Benelli[1)], L. Nemenov[2)]*, M. Pentia[3)], J. Smolik[1)],

[1]Czech Technical University in Prague, Czech Republic
[2]JINR Dubna, Russia
[3]IFIN-HH, National Institute for Physics and Nuclear Engineering, Bucharest, Romania
*Corresponding author.

Abstract

In this work we present the Coulomb effects in the $\pi^+\pi^-$ pair analysis and show the application of these effects in high energy physics investigations. The $\pi^+\pi^-$ pairs were generated in $p-Ni$ interaction at the proton momentum of 24 GeV/c and detected by the DIRAC setup installed on the PS CERN beam. The Coulomb effects (Coulomb correlations) were studied using experimental pair distributions in Q, the relative momentum in the pair center of mass system (c.m.s), and its projections Q_L (longitudinal component) and Q_t (transverse component). The major part of pion pairs $\pi^+\pi^-$ was produced by decay of ρ, ω and Δ and other short-lived sources (Coulomb pairs). In these pairs the significant Coulomb interaction at small Q occurs. The minor part of the pairs are produced if one or both pions arose from long-lived sources like η, η'. In this case the distance between particles will be larger, and the Coulomb interaction in the final state is practically absent. These pairs are defined as non-Coulomb pairs.

The Q, Q_L and Q_t distributions of Coulomb pairs in the c.m.s. were simulated assuming that they are described by the phase space modified by the known Coulomb correlation function $A_C(Q)$. The same spectra of the non-Coulomb pairs were simulated without $A_C(Q)$.

The experimental $\pi^+\pi^-$ pairs were analyzed in the intervals $0 < Q_t < 5$ MeV/c and -20 MeV/c $< Q_L <$20 MeV/c. All the events were divided into nine Q_t intervals, and for each interval the Q_L spectrum was obtained which shows peak around $Q_L = 0$ caused by the Coulomb final state interaction. The full width at half maximum height increases with Q_t from 3 MeV/c for ($0 < Q_t < 0.25$ MeV/c) to 11 MeV/c for (4.0$< Q_t <$5.0 MeV/c). The employed matrix element described the experimental distribution shape as the sum of the Coulomb and non-Coulomb pairs with two free parameters: the ratio of the short-lived and long-lived sources and the normalization constant.

The matrix element contribution to the error in the number of Coulomb pairs is less than 2%. It was shown that with this matrix element, the number of pairs in all Q_t intervals, including the small Q_t, is calculated with the theoretical precision better than 2%. The Q_t values in the center of mass system and in the laboratory system (l.s.) are the same. Therefore the pairs with the minimal Q_t and the maximum total pair momentum in the l.s. have the minimum opening angles θ and the distance D in the same system. The comparison of the simulated number of Coulomb pairs and the experimental number of pairs at small Q_t allows checking and to correcting the detection efficiency for the pairs with small θ (0.05 mrad and smaller) in the laboratory system.

(To be submitted)

1 Introduction

The Coulomb interaction effect was first observed and investigated in the hadron pairs in [1]. The pairs were generated in the reaction

$$p + Ta \longrightarrow \pi^+\pi^- + X \tag{1}$$

at the proton momentum of 70 GeV/c. The pairs ("Coulomb pairs") were described [2] as the product of the pair production matrix element without Coulomb interaction in the final state and the Coulomb correlation function $A_C(Q)$ [3–6], where Q is the relative momentum in the pair center of mass system (c.m.s). This approach was used by analogy with the theoretical description of the Coulomb final state interaction in e^+e^- pair production in photon-nucleus interaction [6]. In both cases the pair production region $\sim 1/m$ (m is the pion or electron mass) is two orders of magnitude smaller than the distance $R \sim 1/\alpha m$ ($\alpha = 1/137$ is the fine structure constant) over which the wave function of the relative motion of the particles changes. It allows one to use the wave function value at $r = 0$. In [1] the Q distribution of $\pi^+\pi^-$ pairs produced in one $p-Ta$ interaction (prompt pairs) divided by the same distribution of the accidental pairs generated at two different production points without interaction in the final state. This ratio $R(Q)_{\rm exp}$ was normalized to unity at the large Q and describes, by definition, the $\pi^+\pi^-$ final state interaction (Coulomb correlation function) dependence on Q . The theoretical ratio $R(Q)_{\rm calc}$ was evaluated with allowance for the full experimental conditions and only Coulomb interaction in the final state. It was shown that $R(Q)_{\rm calc}$ describes the ratio $R(Q)_{\rm exp}$ well in the total analyzed Q interval 0 - 40 MeV/c. The $R(Q)_{\rm exp}$ value increased 6 times when Q decreased from 40 MeV/c to 0.5 MeV/c. The Coulomb correlation function dependences on Q_L (longitudinal component) and Q_t (transverse component) were also well described.

The $\pi^+\pi^-$ prompt pairs distribution in Q_L was analyzed using the following procedure. The experimental accidental pion pair with Q_L was multiplied by $A_C(Q_L)$ to "create" the Coulomb pair. The Coulomb pairs are generated when π^+ and π^- were produced from the decay of ρ, ω, Δ and other short-lived sources. If one or both pions are produced from long-lived sources like η, η' or K_0's, then the distance between particles would be larger and the Coulomb interaction in the final state is almost absent. These pairs were defined as "non-Coulomb" pairs ("decay pairs" in [1]) and their distribution in Q_L was the same as the Q_L spectrum of the accidental pairs. The experimental Q_L distribution was described by the sum of the Coulomb and non-Coulomb pairs. The ratio between the Coulomb and non-Coulomb pairs was taken from the Lund model. The experimental Q_L spectrum was well fitted with one free parameter - the normalization constant.

The Coulomb effects in the $\pi^+\pi^-$ and also $p\pi^-$ pairs were observed and described in [7]

The pairs with the strong Coulomb interaction in the final state create the main background for the observation and investigation of the $\pi^+\pi^-$ atoms [2]. Therefore, to observe $\pi^+\pi^-$ atoms, the Coulomb pair distributions must be described accurately. A detailed description of the $\pi^+\pi^-$ pair spectrum was given in [8], where $\pi^+\pi^-$ atoms were observed for the first time. The $\pi^+\pi^-$ pairs detected in the reaction (1) are generated in the processes shown in Fig.1.

The $\pi^+\pi^-$ atoms produced in the $p-Ta$ interaction are broken up with a large probability while moving in the target, which results in generation of $\pi^+\pi^-$ pairs ("atomic pairs") with the relative momentum Q below 3 MeV/c. The atomic pairs are localized in a small Q interval. This allows one to detect the atomic pairs by accurately describing the Coulomb and non-Coulomb pair Q distributions in a wide interval of the relative momentum and then subtracting these distributions from the total Q spectrum of the all prompt $\pi^+\pi^-$ pairs. The distribution in Q_L and the Q_t components Q_x and Q_y are Gaussian-like and have different standard deviations σ_L, σ_X.and σ_Y. Therefore, the prompt $\pi^+\pi^-$ distribution was

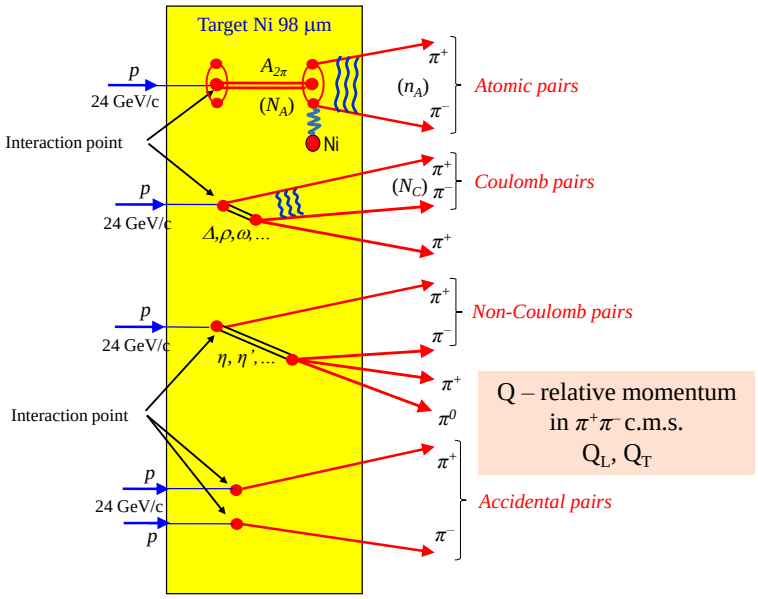

Fig. 1: The atomic, Coulomb, non-Coulomb and accidental pair production processes. The wave lines denote the Coulomb interaction.

analyzed using the parameter

$$F = \sqrt{\left(\frac{Q_L}{\sigma_L}\right)^2 + \left(\frac{Q_X}{\sigma_X}\right)^2 + \left(\frac{Q_Y}{\sigma_Y}\right)^2} \tag{2}$$

The Coulomb and non-Coulomb pair spectra as a function of F were obtained in the same way as the pair distributions in Q_L described above. It was shown that the prompt pair spectrum in F in the interval 0-40 MeV/c is well described as the sum of the Coulomb and non-Coulomb distribution pairs with two free parameters: the normalization constant and the ratio between the Coulomb and non-Coulomb pairs.

A more precise description of the Coulomb and non-Coulomb pairs was done in the DIRAC experiment at CERN to measure the $\pi^+\pi^-$ atom lifetime and the $\pi\pi$ scattering length [9]. In this experiment $\pi^+\pi^-$, π^+K^-, π^-K^+, K^+K^- and $p\overline{p}$ pairs were generated in the reaction

$$p + Ni \longrightarrow h^+h^- + X \tag{3}$$

with the proton momentum of 24 GeV/c.

The Coulomb pair Q distribution in the c.m.s. was simulated assuming that they are described by the phase space modified by the Coulomb correlation function $A_C(Q)$. The same spectrum of the non-Coulomb pairs was simulated without $A_C(Q)$. The c.m.s. pion momenta were transformed in the l.s. using the experimental total momentum spectrum of the $\pi^+\pi^-$ pairs. The difference between the total momentum distribution of the Coulomb and non-Coulomb pairs was taken into account using FRITIOF-6. This approach allowed a good description of Q and Q_L. In the second DIRAC experiment [10] more experimental data were analyzed. Coulomb pair simulation involved the Coulomb and strong $\pi^+\pi^-$ interaction in the final state and the influence of the nonpoint-like pair production on the spectrum shape [11] The sources of the nonpoint-like Coulomb pair production were investigated in [12]. A new procedure [13, 14] was used that allowed more accurately taking into account the difference between the

total momentum distributions of the Coulomb and non-Coulomb pairs in the l.s. This analysis enabled good description of the Coulomb pair distribution in Q_L and Q_t in the intervals 0-15 MeV/c and 0-5 MeV/c respectively.

The DIRAC setup was upgraded to identify and investigate $\pi^+\pi^-$, π^+K^-, π^-K^+, K^+K^- and $p\bar{p}$ pairs [15]. In the dedicated experiment [16], the π^+K^- and π^-K^+ Coulomb, non-Coulomb and atomic pairs were accurately described. The $\pi^+\pi^-$ pairs were the background events in those works. An improved version of the simulation procedure SP-1 and a more accurate setup geometry tuning were used [17].
It made it possible to observe for the first time the π^+K^- and π^-K^+ atoms, measure their lifetime and evaluate the πK scattering length. In all those investigations the $\pi^+\pi^-$ pairs were the background processes used to check the setup tuning [17]. The simulation procedure used in the present work is SP-2.

The present work deals with investigation of the $\pi^+\pi^-$ pairs detected by the upgraded DIRAC setup [15] in which new detectors were installed to suppress K mesons, protons and antiprotons. It allowed to suppress K^-K^+ and $p\bar{p}$ pairs particle admixture in the pion pair data.

2 Setup and experimental conditions

The aim of the magnetic two-arm vacuum spectrometer [15, 18–20] (Fig. 2) is to detect and identify K^+K^- , $\pi^+\pi^-$, π^-K^+, and π^+K^- pairs with small Q. The structure of K^+K^- and $\pi^+\pi^-$ pairs downstream the magnet is approximately symmetric. The 24 GeV/c primary proton beam, extracted from the CERN PS, hit a Ni target of (108 ± 1)μm thickness or $7.4 \cdot 10^{-3} X_0$.

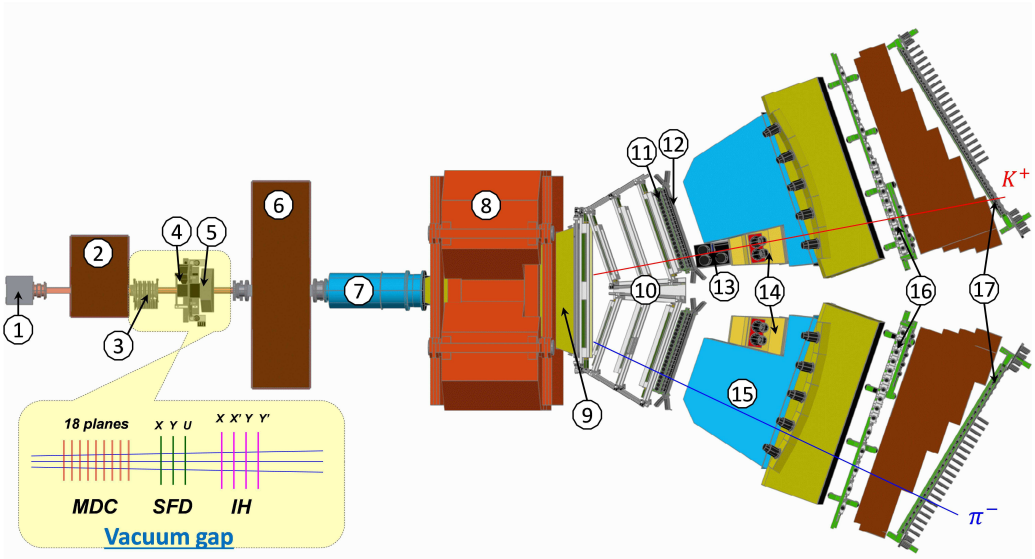

Fig. 2: General view of the DIRAC setup (1 – target station; 2 – first shielding; 3 – micro drift chambers (MDC); 4 – scintillating fiber detector (SFD); 5 – ionization hodoscope (IH); 6 – second shielding; 7 – vacuum tube; 8 – spectrometer magnet; 9 – vacuum chamber; 10 – drift chambers (DC); 11 – vertical hodoscope (VH); 12 – horizontal hodoscope (HH); 13 – aerogel Cherenkov (ChA); 14 – heavy gas Cherenkov (ChF); 15 – nitrogen Cherenkov (ChN); 16 – preshower (PSh); 17 – muon detector (Mu).

The axis of the secondary channel is inclined relative to the proton beam by 5.7° upward. The solid angle of the channel is $\Omega = 1.2 \cdot 10^{-3}$ sr. Secondary particles propagate mainly in vacuum to the Al foil $(7.6 \cdot 10^{-3} X_0)$ at the exit of the vacuum chamber, which is installed between the poles of the dipole magnet (B_{max} = 1.65 T and BL = 2.2 Tm). In the vacuum channel gap, 18 planes of the Micro Drift Chambers (MDC) and (X, Y, U) planes of the Scintillation Fiber Detector (SFD) were installed to measure both the

particle coordinates ($\sigma_{SFDx} = \sigma_{SFDy} = 60$ µm, $\sigma_{SFDu} = 120$ µm) and the particle time ($\sigma_{tSFDx} = 380$ ps, $\sigma_{tSFDy} = \sigma_{tSFDu} = 520$ ps). The total matter radiation thickness between the target and the vacuum chamber amounts to $7.7 \cdot 10^{-2} X_0$.

Each spectrometer arm is equipped with the following subdetectors [15]: drift chambers (DC) to measure particle coordinates with approximately 85 μm precision and to evaluate the particle path length; a vertical hodoscope (VH) to determine particle times with 110 ps accuracy for identification of equal mass pairs via the time of flight (TOF) between the SFDx plane and the VH; a horizontal hodoscope (HH) to select particles with a vertical distance less than 75 mm (Q_Y less than 15 MeV/c) in the two arms; an aerogel Cherenkov counter (ChA) to distinguish kaons from protons; a heavy gas (C_4F_{10}) Cherenkov counter (ChF) to distinguish pions from kaons and protons; a nitrogen Cherenkov (ChN) and preshower (PSh) detectors to identify e^+e^-; an iron absorber and a two-layer scintillation counter (Mu) to identify muons. In the "negative" arm, no aerogel counter was installed, because the number of antiprotons is small compared to K^-.

Pairs of oppositely charged particles generated in one $p-Ni$ interaction (prompt pairs) and accidentals produced in two different interactions in the time interval ± 20 ns are selected by requiring a 2-arm coincidence (ChN in anticoincidence) with the coplanarity restriction (HH) in the first-level trigger. The second-level trigger selects events with at least one track in each arm by exploiting the DC-wire information (track finder). Particle pairs $\pi^- p$ ($\pi^+ \bar{p}$) from Λ ($\bar{\Lambda}$) decay were used for spectrometer calibration, and e^+e^- pairs were employed for general detector calibration.

3 Data processing

The collected events were analyzed with the DIRAC reconstruction program ARIANE [21].

3.1 Tracking

Only events with one or two particle tracks in the DC of each arm are processed. The event reconstruction is performed according to the following steps [16]:

- One or two hadron tracks are identified in the DC of each arm with hits in VH, HH and PSh slabs and no signal in ChN and Mu.
- Track segments reconstructed in the DC are extrapolated backward to the beam position in the target, using the transfer function of the dipole magnet and the program ARIANE. This procedure provides approximate particle momenta and the corresponding points of intersection in the MDC, SFD and IH.
- Hits are searched for around the expected SFD coordinates in the region ± 1 cm corresponding to (3–5) $\sigma_{\rm pos}$ defined by the position accuracy with allowance for the particle momenta. To identify the event when two particles crossed the same SFD column, the double ionization in the corresponding IH slab was requested.

The momentum of the positively or negatively charged particle is refined to match the X-coordinates of the DC tracks as well as the SFD hits in the X- or U-plane, depending on the presence of hits. In order to find the best 2-track combination, the two tracks may not use a common SFD hit in the case of more than one hit in the proper region. In the final analysis, the combination with the best χ^2 in the other SFD planes is kept.

3.2 Setup tuning with Λ and $\bar{\Lambda}$ particles

In order to check the general geometry of the DIRAC experiment, Λ and $\bar{\Lambda}$ particles decaying into $p\pi^-$ and $\pi^+\bar{p}$ in our setup were used [16]. After the setup tuning the weighted average of the experimental

Λ mass over all runs, $M_\Lambda^{\mathrm{DIRAC}} = (1.115680 \pm 2.9 \cdot 10^{-6})$ GeV/c^2, agrees very well with the PDG value, $M_\Lambda^{\mathrm{PDG}} = (1.115683 \pm 6 \cdot 10^{-6})$ GeV/c^2. The weighted average of the experimental $\bar{\Lambda}$ mass is $M_{\bar{\Lambda}}^{\mathrm{DIRAC}} = (1.11566 \pm 1 \cdot 10^{-5})$ GeV/c^2. This demonstrates that the geometry of the DIRAC setup is well described.

The width of the Λ mass distribution allows testing the momentum and angular resolution of the setup in the simulation. Table 1 shows a good agreement between the simulated and experimental Λ widths in DATA2 and DATA3. A further test consists in comparing the experimental Λ and $\bar{\Lambda}$ widths.

Table 1: The Λ width in GeV/c^2 for the experimental and MC data and the $\bar{\Lambda}$ width for the experimental data.

	Λ width (data) GeV/c^2	Λ width (MC) GeV/c^2	$\bar{\Lambda}$ width (data) GeV/c^2
DATA2	$4.42 \cdot 10^{-4} \pm 7.4 \cdot 10^{-6}$	$4.42 \cdot 10^{-4} \pm 4.4 \cdot 10^{-6}$	$4.5 \cdot 10^{-4} \pm 3 \cdot 10^{-5}$
DATA3	$4.41 \cdot 10^{-4} \pm 7.5 \cdot 10^{-6}$	$4.37 \cdot 10^{-4} \pm 4.5 \cdot 10^{-6}$	$4.3 \cdot 10^{-4} \pm 2 \cdot 10^{-5}$

The average value of the correction which was introduced in the simulated width is $1.00203 \pm 0.00191 \cdot 10^{-3}$. To obtain this correction, nonsignificant corrections were introduced in the l.s. particle momenta.

3.3 Event selection

The processed events were collected in the DATA1, DATA2 and DATA3 samples. Equal-mass pairs contained in the selected event sample are classified into three categories: $\pi^+\pi^-$, K^+K^-, and $p\bar{p}$ pairs.

The classification is based on the TOF measurement [22] for the distance between the SFD X-plane and the VH of about $11m$. For pairs with total momenta range-mg from 3.8 to 8 GeV/c, additional information from the Heavy Gas Cherenkov (ChF) counters (Section 2) is used to better separate $\pi^+\pi^-$ from K^+K^- and $p\bar{p}$ pairs. The ChF counters detect pions in this region with (95–97)% efficiency [23], whereas kaons and protons (antiprotons) do not generate any signal.

4 Description of $\pi^+\pi^-$ pair production and the simulation procedure

The experimental data (Data1, Data 2 and Data 3) were obtained during three different runs.

The experimental distributions of the Coulomb and non-Coulomb pairs on the relative momentum Q and its components were compared with the corresponding simulated spectra.

The simulated Coulomb $\pi^+\pi^-$ spectra in the pair c.m.s. were calculated using the relation

$$\frac{dN}{dQ_i} = \left|M_{\mathrm{prod}}\right|^2 F(Q_i) A_C(Q_i) \tag{4}$$

where Q_i is Q, Q_L or Q_t, M_{prod} is the production matrix element without Q dependence in the investigated Q interval, $F(Q_i)$ is the phase space and $A_C(Q)$ is the Coulomb correlation function

$$A_C(Q) = \frac{2\pi m_\pi \alpha / Q}{1 - exp(-2\pi m_\pi \alpha / Q)} \tag{5}$$

with allowance for the Coulomb final state interaction (FSI).

For the small and the large Q the respective Coulomb correlation function values are

$$A_C = 2\pi m_\pi \alpha / Q \quad \text{and} \quad A_C = 1 \tag{6}$$

In accordance with formula (4), the pair distribution in Q_L in the Qt interval from $Q_{t\,min}$ to $Q_{t\,max}$ is:

$$\frac{dN}{dQ_L} = \int_{Q_{t\,min}}^{Q_{t\,max}} Q_t A_C(Q)\, dQ_t \qquad \text{with} \qquad Q = \sqrt{Q_t^2 + Q_L^2} \tag{7}$$

In the results obtained with formula (4), involves corrections were introduced to take into account the strong interaction in the final state [11]. and nonpoint-like production of Coulomb pairs [12].

These corrections decrease the number of the Coulomb pairs calculated by formula (4) in the Q interval 0-3 MeV/c. The maximum distribution decrease is 3% at Q=0 MeV/c. The reduction in the number of the Coulomb pairs at small Q is important for the evaluation of the number of the atomic pairs. The total number of the Coulomb pairs obtained by formula (4), can be used without corrections using the fitting procedure excluding the Q interval less than 2 MeV/c. In this case the relative error in the total number of the Coulomb pairs will be less than 1%.

The same simulation was done for the non-Coulomb $\pi^+\pi^-$ pairs using formula (4) without the correlation function $A_C(Q)$. The Q_L distributions of non-Coulomb and accidental pairs are the same. Therefore, in all analyses presented below the numbers of non-Coulomb pairs include the admixture of accidental pairs.

To calculate the momenta of the pair particles in the laboratory system, the l.s. pair momentum added to the c.m.s. taking into account the difference between the total momentum distributions of the Coulomb and non-Coulomb pairs in l.s. [13, 14]. This allows calculating the momenta $\vec{P}^+$ and $\vec{P}^-$ of the π^+ and π^- in l.s. and their total momentum $\vec{P} = \vec{P}^+ + \vec{P}^-$. By using the dedicated code GEANT-DIRAC, the simulated pairs are propagated through the setup with allowance for the multiple scattering and the response of the detectors. Before reaching the magnet the $\pi^+\pi^-$ crosses the Scintillator Fiber Detector (SFD) and the Ionization Detector (ID).

The distance D between the two particles in l.s. decreases with Q_t and for the small D in this experiment the coordinate scintillation fiber detector with the some probability cannot distinguish a one-particle hit from a two-particle hit. In this case, the amplitude is measured in the ionization detector. If the amplitude is higher than some threshold, this event is considered as the two-particle hit. Introduction of the threshold results in rejecting the part of the pairs and decreasing their detection efficiency ε. This decrease begins with D reducing below 0.8 mm in the x and y projections; the corresponding pair opening angle projections are 0.28 mrad. After the spectrometer magnet, only events with one or two tracks per arm are selected.

On the basis of the information from the detectors, the events were reconstructed by the ARIANE code and processed as experimental pairs. The simulated event distribution in $\vec{P}_{\text{lab}}$ was tuned by requiring that the Coulomb and non-Coulomb pairs fit the experimental $\pi^+\pi^-$ pair spectrum in $\vec{P}_{\text{exp}} = \vec{P}^+_{\text{exp}} + \vec{P}^-_{\text{exp}}$ where $\vec{P}^+_{\text{exp}}$ and $\vec{P}^-_{\text{exp}}$ are the experimental l.s. momenta of π^+ and π^-. After this the Q_L, Q_t and Q distributions of the simulated events were calculated and compared with the experimental spectra.

5 Analysis of experimental Q_L distributions of $\pi^+\pi^-$ pairs and measurement of the number of Coulomb and non-Coulomb pairs

The experimental prompt (without accidentals) $\pi^+\pi^-$ pair distributions in Q_L were separately fitted in three data samples by the sum of the simulated Coulomb and non-Coulomb pair distributions in nine Q_t intervals: 0-0.25 (1), 0.25-0.5, 0.5-075, 0.75-1, 0-1 (2), 1-2 , 2-3 (3), 3-4 and 4-5 MeV/c (4). Four of them are marked by numbers in parentheses for further references.

The ratio between these pairs in each interval was the free parameter. The fitting interval -20 MeV/c <

$Q_L < 20$ MeV/c did not include the region -2 MeV/$c < Q_L < 2$ MeV/c which involves atomic pairs having a different shape of the Q_L and Q_t spectra. The number of the simulated events for each data sample is an order of magnitude larger than the number of the corresponding experimental events.

Figure 3 shows the sum of three samples of experimental and fitting distributions in intervals (1)-(4). Also, the fitting distributions of the Coulomb and non-Coulomb pairs are presented separately. The excess events in the interval -2 MeV/$c < Q_L < 2$ MeV/c are due to the atomic pairs. The experimental Coulomb pair spectrum shows the peak around $Q_L = 0$. The full width at half maximum increases with Q_t, and for Q_t intervals 1, 2, 3 and 4 the width values are 3.4 MeV/c, 4 MeV/c, 6.5 MeV/c and 11 MeV/c respectively. They were obtained by measuring the histogram parameters.

The Coulomb pair distributions in Q_L for Q_t intervals (1)-(4) at the pair production point were evaluated using formula (4) and are presented in Fig.4. The full width at half maximum for the four Q_t intervals are 1.0 MeV/c, 1.2 MeV/c, 6.4 MeV/c and 10.6 MeV/c respectively. The same values for the experimental distributions in the Q_t interval 0-1 MeV/c are significantly larger. In the DIRAC experiment the main contribution to the width increase comes from the multiple scattering in the target. The multiple scattering in the detectors and the accuracy of the particle coordinate measurements are less important.

Table 1. shows the fitting procedure χ^2/ndf values for three data samples and five Q_t intervals

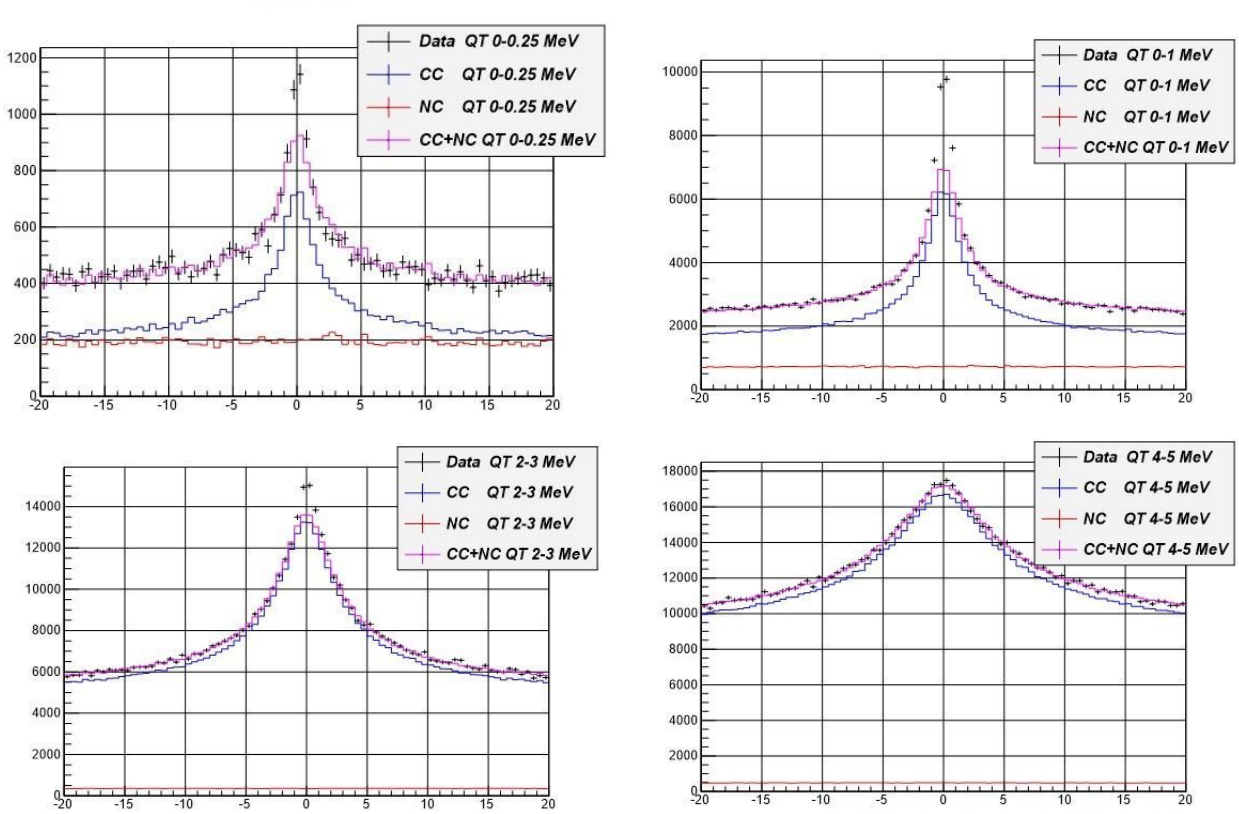

Fig. 3: The experimental Q_L distributions of the prompt Coulomb, non-Coulomb and atomic pairs (sum of three data samples) for the Q_t intervals 0.0-0.25 MeV/c, 0.0-1.0 MeV/c, 2.0-3.0 MeV/c and 4.0-5.0 MeV/c. The histogram is the corresponding sum of the simulated Coulomb and non-Coulomb pairs fitting the experimental spectrum in the total Q_L interval not including the region -2 MeV/$c < Q_L <$2 MeV/c where atomic pairs are present. The fitting histograms that describe the Coulomb (blue) and non-Coulomb (red) experimental pairs are presented as separate histograms. It is seen that selection of the experimental Coulomb pairs in different Q_T intervals allows one to obtain Q_L distributions with the peaks and change the peak widths. The pairs contribution above the fitting histogram in the interval -2 MeV/$c < Q_L <$2 MeV/c is due to the atomic pairs.

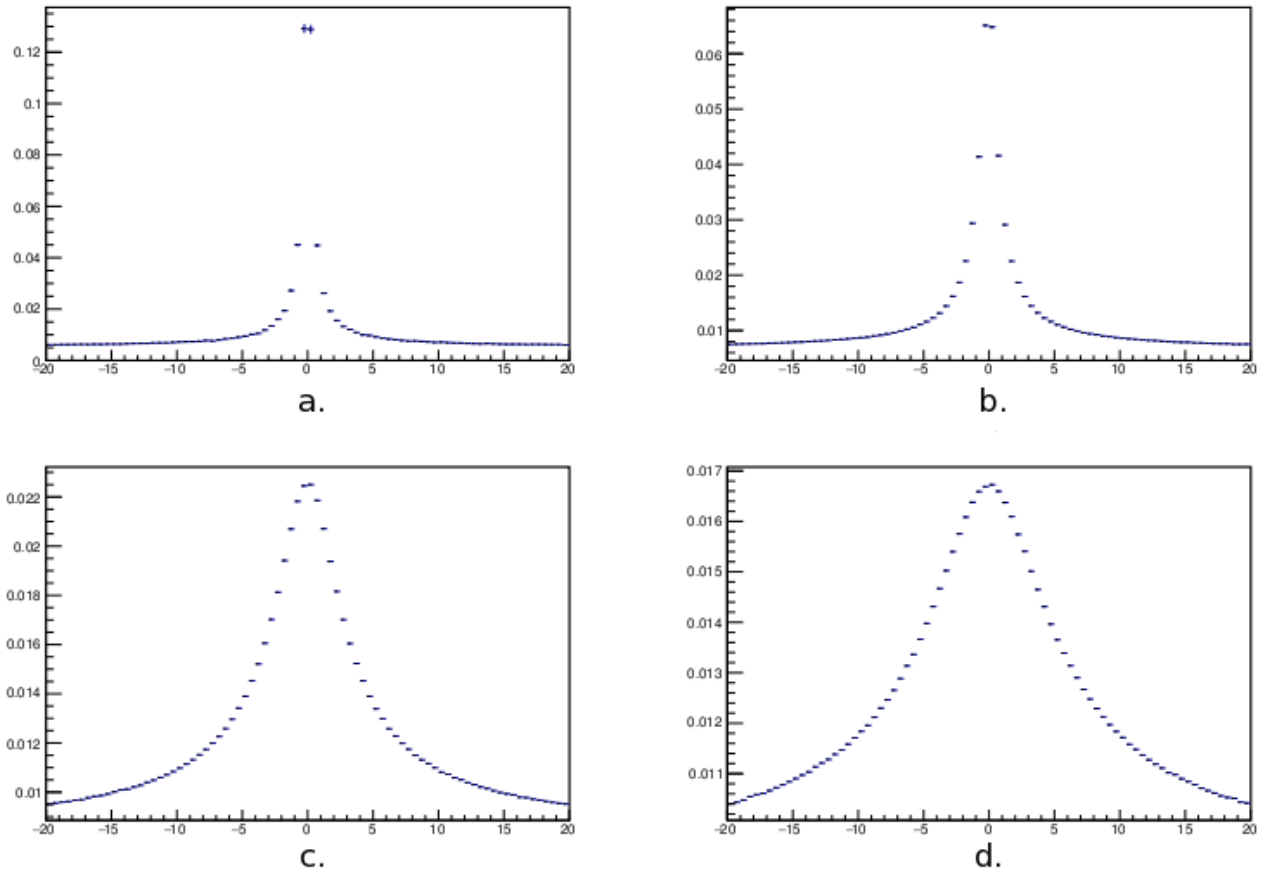

Fig. 4: The simulated Q_l distributions of $\pi^+\pi^-$ Coulomb pairs at the production point for Q_t intervals: a. 0-0.25 MeV/c, b. 0-1 MeV/c, c. 2-3 MeV/c, d. 4-5 MeV/c. All distributions are normalized to unity.

Table 2:

ΔQ_t (MeV/c)	0-1.0	1.0-2.0	2.0-3.0	3.0-4.0	4.0-5.0
χ^2/ndf values					
Data 1	1.35	1.09	1.12	1.14	1.41
Data 2	1.45	0.90	1.29	0.90	1.19
Data 3	1.20	1.46	1.09	1.46	0.91

The χ^2/ndf values for four other Q_t intervals are presented in Table 2.
The probability density function (PDF) has the maximum around $\chi^2/ndf = 1$ and decreases by half for $\chi^2/ndf = 0.83$ and 1.17. Out of 27 χ^2/ndf values 22 are in the interval 0.83-1.34. Five χ^2/ndf values are larger than 1.34. But in each Q_t interval that has a large χ^2/ndf value for one data sample there are always two χ^2/ndf values for the other data samples in the interval 0.83-1.34. The shape of the experimental Q_L distributions strongly change with increasing Q_t. But it is seen from Tables 2 and 3 that the simulated distributions fit these spectra well in all Q_t intervals.

Table 4 presents $NC_{\rm exp}(\Delta Q_t)$, experimental numbers of Coulomb pairs in the interval ΔQ_t, and their relative errors for the Data 3 sample.
Table 5 shows relative errors in the Q_t interval 0-1 MeV/c.
It is seen that the relative precision of the number of Coulomb pairs decreases with decreasing Q_t because the background level becomes higher and the number of Coulomb pairs becomes smaller. The relative

Table 3:

ΔQ_t (MeV/c)	0-0.25	0.25-0.5	0.5-0.75	0.75-1.0
χ^2/ndf values				
Data 1	1.12	1.17	1.12	0.94
Data 2	1.30	1.10	1.06	1.10
Data 3	1.78	1.25	1.00	1.29

Table 4:

ΔQ_t (MeV/c)	0-1.0	1.0-2.0	2.0-3.0	3.0-4.0	4.0-5.0
$NC_{\mathrm{exp}}(\Delta Q_t)$	75200	137900	215900	298000	368600
relative error	3.6%	2.2%	1.9%	1.7%	1.8%
$NC_{\mathrm{calc}}(\Delta Q_t)$	75720	140030	217330	294760	367190

Table 5:

ΔQ_t (MeV/c)	0-0.25	0.25-0.5	0.5-0.75	0.75-1.0
$NC_{\mathrm{exp}}(\Delta Q_t)$	9460	21760	21130	25750
relative-error	10.5%	6.3%	6.2%	5%
$NC_{\mathrm{calc}}(\Delta Q_t)$	7890	19480	23190	25160

errors in the Data 2 sample are the same as in the Data 3 sample. The relative errors in the number of Coulomb pairs depend on the experimental distribution shape, statistical errors and simulated distribution precision which is defined by the setup description quality and the theoretical accuracy of formula (4) with the corrections. Therefore, the relative errors of the number of Coulomb pairs give the minimum accuracy of the theoretical approach. A conclusion that can be drawn from these two analyses is that the theoretical approach using formula (4) allows one to describe the experimental distributions in Q_L and to obtain the number of Coulomb pairs with the precision better than 2% in Q_t interval 0-5 MeV/c.

The performed analysis allows the ratio between the pairs generated by short-lived sources like ρ, ω, K*... and the pairs generated by long-lived sources like η, η' to be measured with a precision about 2% and the evaluated results to be compared with the theoretical predictions.

6 Analysis of experimental Q_t distributions of Coulomb pairs

In section 5 it was shown that the simulated distributions based on the relation (4) describe well Q_L distributions of Coulomb pairs for nine fixed Q_t intervals. In this section will be shown that formula (4) also describes the Q_t distribution of the experimental Coulomb pairs with Q_L belonging to the interval -20 MeV/c $< Q_L <$ 20 MeV/c. If Q_t decreases, the number of pairs with the small distance D between the tracks increases in the corresponding Q_t intervals. For these pairs the detection efficiency ε has a strong dependence on D (see section 4), and the errors in ε give rise to distortion of the number of simulated events and their greater difference from the number of experimental pairs. The analysis will also allow checking the accuracy of the ε dependence on D used in the DIRAC simulation procedure.

The fitting procedure described in section 5 was applied to the experimental Q_L distribution of the pairs (fitting interval -20 MeV/c $< Q_L <$ 20 MeV/c, excluding the region -2 MeV/c $< Q_L <$ 2 MeV/c) with the total Q_t interval 0-5 MeV/c to obtain $|M_{\mathrm{prod}}|^2$ for the simulated events. The results of the analysis are presented in Table 6.

Table 6:

	Data 1	Data 2	Data 3
Number of Coulomb pairs	710300	1108400	1095000
Relative errors	1.2%	0.92%	0.92%
χ^2/ndf	1.4	1.01	1.4

It is seen that formula (4) describes well all the experimental data in the Q_t interval 0-5 MeV/c with an average precision better than 1%.

The simulated distributions were obtained using formula (4) in which $|M_{\rm prod}|^2$ does not depend on Q. The analysis allows one to check it. The simulated Q_L distribution of the Coulomb and non-Coulomb pairs in each data sample was divided by the same experimental spectrum. The sum of the ratios for the three data samples as function of Q_L are presented in Fig.5. It is seen that for all the Q_L values in the fitting intervals (excluding region $\pm$ 2 MeV/c) the ratios are around unity. The left and the right sides of the plotted ratios were fitted independently. The average ratio values for the negative and positive Q_L are 1.0000 ± 0.0021 and 1.0009 ± 0.0021 respectively, demonstrating that the existing data are not sensitive to the Q dependence of the $|M_{\rm prod}|^2$.

The $|M_{\rm prod}|^2$ evaluation allows calculating $NC_{\rm calc}(\Delta Q_t)$, the expected number of the simulated Coulomb pairs in each of the ΔQ_t intervals analyzed in section 5. The thus obtained $NC_{\rm calc}(\Delta Q_t)$ were compared with the $NC_{\rm exp}(\Delta Q_t)$ evaluated in section 5 by the fitting procedure in the same ΔQ_t intervals.

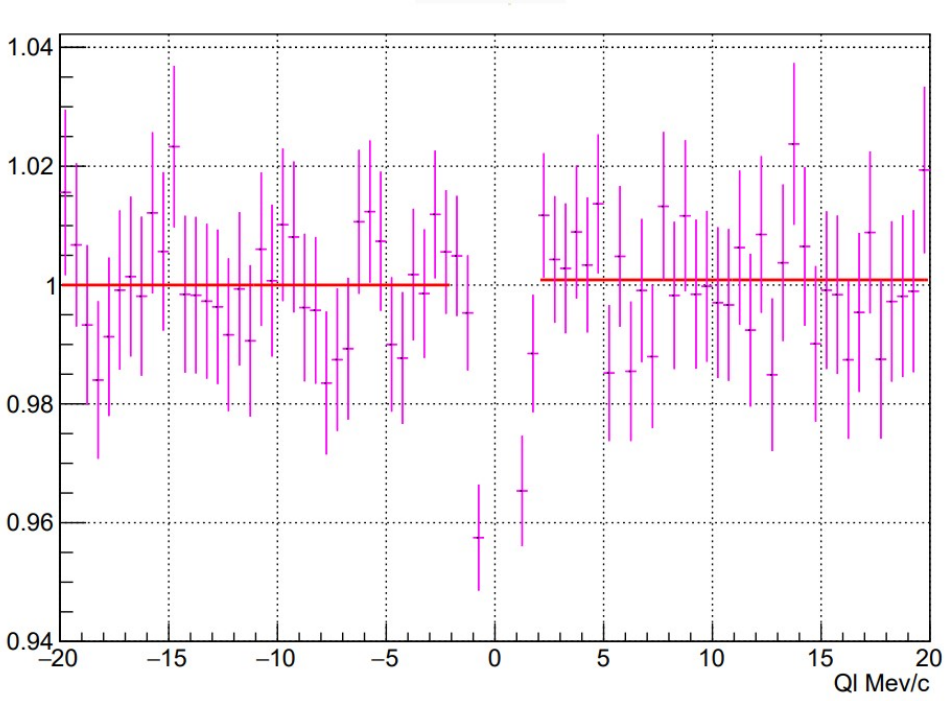

Fig. 5: The simulated Q_L distribution of the Coulomb and non-Coulomb pairs in each data sample was divided by the same experimental spectrum. The sum of the ratios for the three data samples is presented as a function of Q_L. In the intervals of the positive and negative Q_L (excluding region $\pm$ 2MeV/c) the points were fitted independently. It is seen that in the left and right intervals the average ratios are unity, demonstrating that the existing data are not sensitive to the Q dependence of the $|M_{\rm prod}|^2$ from formula (4).

The results of the Data 3 analysis for nine ΔQ_t intervals are presented in Fig. 6. It is seen that the

differences between these numbers in all nine Q_t intervals are less than two standard deviations. The same good agreement is for the Data1 and Data2 samples. It demonstrates that formula (4) describes the experimental data in all Q_t and Q_L intervals with the precision better than 2% as was established in section 5 for Q_L distribution.

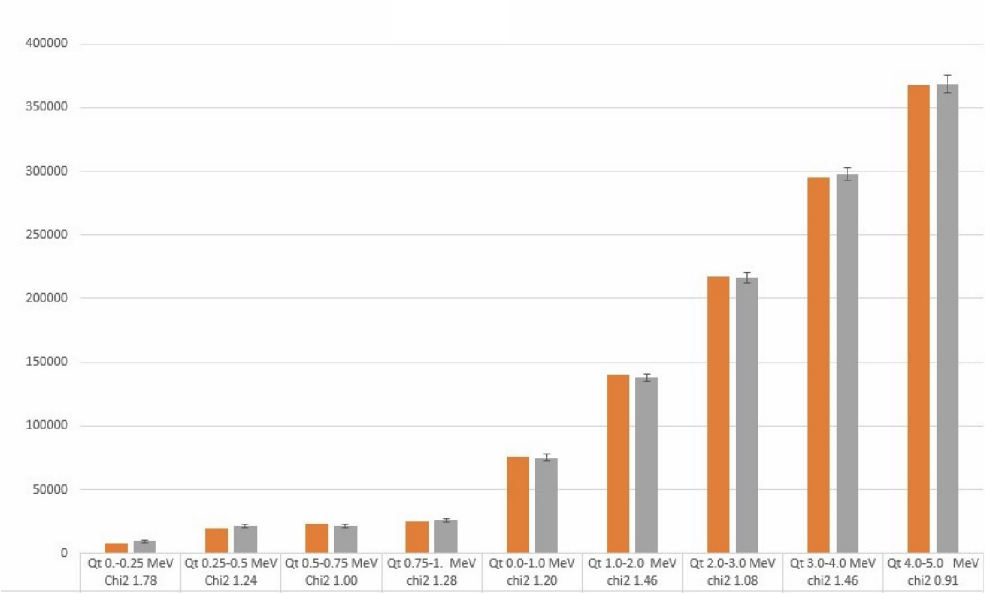

Fig. 6: The experimental numbers of Coulomb pair $NC_{\rm exp}(\Delta Q_t)$ for different Q_t intervals (gray). The calculated numbers of Coulomb pair $NC_{\rm calc}(\Delta Q_t)$ for the same Q_t intervals (brown).

It is seen that in all nine Q_t intervals there is a good agreement between $NC_{\rm exp}$ and the number of the simulated events $NC_{\rm calc}$ evaluated with relation (4). Tables 4 and 5 presented $NC_{\rm exp}$ and $NC_{\rm calc}$.

Figure 6 shows that the main contribution to $|M_{\rm prod}|^2$ comes from the pairs with large Q_t. The distance D of these pairs is large and their detection efficiency is well defined. The agreement between $NC_{\rm exp}(\Delta Q_t)$ and $NCcalc(\Delta Q_t)$ for pairs with Q_t less than 0.5 MeV/c shows that the ε dependence on D at small distance between tracks was taken into account correctly.

7 The values of the angles between two tracks in the laboratory system

The Q_t values in the center of mass system and in the laboratory system are the same. Therefore, the pairs with the minimal Q_t and the maximum total pair momentum in the l.s. have the minimum opening angles θ and the distance D in the same system. Total momenta of the experimental pairs are found mainly in the interval 2.4-8 GeV/c with the average value of about 4 GeV/c.

In interval (4) the average Q_t value is 4.5 MeV/c. The angle between two particles in the l.s. at this Q_t and the average pair total momentum is 2 mrad. The average Q_t value in interval (1) is around 0.12 MeV/c, and the opening angle for the average total pair momentum is 0.05 mrad. The contributions of the pairs with smaller Q_t and larger total momentum allows checking the detection efficiency for the pairs with the opening angles about 0.01 mrad. The distribution with large Q_t allows checking and correcting the simulation procedure for the pairs with large opening angles in the l.s. The detection efficiency of these pairs is the product of the well-known efficiencies of the single particle detection. After the tuning of the simulation procedure and the evaluation of the $|M_{\rm prod}|^2$ value using these pair distributions, the expected numbers of the simulated Coulomb pairs in the intervals with small Q_t can be calculated with the theoretical accuracy better than 2%. The comparison of the numbers of the simulated pairs $NC_{\rm calc}$

and the numbers of the experimental pairs $NC_{\rm exp}$, allows checking and correcting the detection efficiency for the pairs with the small distance D.

8 Conclusion

In this work the Coulomb effects in the $\pi^+\pi^-$ pairs were studied and their application in the high-energy physics investigations is justified. The $\pi^+\pi^-$ pairs were generated in pNi interactions with the proton momentum of 24 GeV/c and detected by the DIRAC setup installed on the CERN PS beamline in the East Hall. The experimental data samples DATA1, DATA2 and DATA3 were obtained in three different runs. Each data sample was independently processed using proper geometry tuning and detector response analysis. The Coulomb effects (Coulomb correlations) were studied using the experimental pair distributions in Q, the relative momentum in the pair c.m.s., and its longitudinal (Q_L) and transverse (Q_t) projections. The major part of the pion pairs were generated when π^+ and π^- were produced in decays of ρ, ω, Δ and other short-lived sources (Coulomb pairs). In these pairs at small Q, the significant Coulomb interaction in the final state arises, and the pair yield increases with decreasing Q . The minor part of the pairs is produced if one or both pions result from long-lived sources, such as η, η' (non-Coulomb pairs). In this case the distance between particles would be much larger than the Bohr radius of the $\pi^+\pi^-$ atom, and the Coulomb interaction in the final state is almost absent.

The experimental $\pi^+\pi^-$ pair distributions were analyzed in the intervals $0 < Q_t < 5$ MeV/c and -20 MeV/c $< Q_L <$ 20 MeV/c using the sum of the corresponding simulated Coulomb and non-Coulomb pair distributions. The simulated spectra of the Coulomb $\pi^+\pi^-$ pairs in the c.m.s. were obtained with the simple (relation (4)) matrix element: the product of the phase space and the well-known Coulomb correlation function $A_C(Q)$. Also, corrections were introduced in formula (4) to take into account the strong $\pi\pi$ interaction in the final state and the nonpoint-like production of Coulomb pairs. These corrections decrease the number of Coulomb pairs calculated by relation (4) in the Q interval 0-3 MeV/c by about 2% while in other intervals this effect is much smaller. The non-Coulomb $\pi^+\pi^-$ pairs was simulated using formula (4) without the correlation function $A_C(Q)$.

To calculate the momenta of the simulated pair particles in the laboratory system, the l.s. pair momentum was added to the c.m.s. system with allowance for the difference between the total momentum distributions of the Coulomb and non-Coulomb pairs in the l.s. By using the dedicated GEANT-DIRAC code, the simulated pairs were generated and propagated through the setup, with account taken of the multiple scattering and the detector response. Before reaching the magnet, the $\pi^+\pi^-$ pairs crossed the Scintillator Fiber Detector (SFD) and the Ionization Detector (ID). The combination of the SFD and the IH detect pairs with the efficiency ε depending the distance D between particles: ε decreases with decreasing D to less than 0.8 mm in the x or y projections; the corresponding pair opening angle projections are 0.28 mrad.

On the basis of the information from the detectors, the events were reconstructed by the ARIANE code and processed as experimental pairs. All experimental events were divided into nine Q_t intervals: 0-0.25 , 0.25-0.5, 0.5-075, 0.75-1, 0-1 , 1-2 , 2-3 , 3-4 and 4-5 MeV/c. In each interval Q_L spectra were obtained which showed peaks around $Q_L = 0$ caused by the Coulomb final state interaction (Fig.3).

Each distribution was fitted (section 5) by the sum of the simulated Coulomb and non-Coulomb pairs with two free parameters: the ratio between the short-lived and long-lived sources and the normalization constant. The fitting interval did not include the region -2MeV/c $< Q_L <$ 2 MeV/c which involved atomic pairs that arose from the breakup of $\pi^+\pi^-$ atoms in the target (Fig.1) and had a different shape of the Q_L and Q_t spectra.

Nine experimental distributions in all three data samples were described well. The full width at half maximum increases with Q_t and is 3.4 MeV/c ($0 < Q_t <$ 0.25 MeV/c), 4 MeV/c ($0 < Q_t <$ 1 MeV/c),

6.5 MeV/c ($2 < Q < 3$ MeV/c) and 11 MeV/c ($4 < Q_t <$ 5MeV/c).

It was shown that the matrix element contribution to the error in the number of Coulomb pairs is less than 2%. The fitting procedure described in section 5 was applied to the experimental pair distribution in Q_L with Q_t from the total interval 0-5 MeV/c to evaluate $|M_{\rm prod}|^2$ in formula (4). It allowed calculation of $NC_{\rm calc}(\Delta Q_t)$, the expected number of the simulated Coulomb pairs in each of the nine ΔQ_t intervals. The thus obtained $NC_{\rm calc}(\Delta Q_t)$ were compared with $NC_{\rm exp}(\Delta Q_t)$ evaluated by the fitting procedure in the same ΔQ_t intervals.

The results of the Data 3 analysis for nine ΔQ_t intervals are presented in Fig.6. It is seen that in all nine Q_t intervals there is good agreement between $NC_{\rm exp}$ and the number of the simulated events $NC_{\rm calc}$. It was shown (Tables 4 and 5) that the difference between $Nc_{\rm exp}(Q_t)$ and $NC_{\rm calc}$ in nine Q_t intervals is less than two standard deviations.

The same good agreement is for the Data1 and Data 2 samples. It demonstrates that formula (4) describes the experimental Q_t and Q_L distributions of Coulomb pairs with the precision better than 2% and the dependence of the efficiency ε on the distance D between the particles is taken into account correctly.

The Q_t values in the center of mass system and in the laboratory system are the same. Therefore, the pairs with the minimal Q_t and the maximum total pair momentum in the l.s. have the minimum opening angles θ and the minimum distance D in the same system. The experimental pair total momenta are mainly in the interval 2.4 GeV/c- 8 GeV/c with the average value of about 4 GeV/c.

At Q_t = 4.5 MeV/c (interval 4.0-5.0 MeV/c) and the total momentum of 4.0 GeV/c the angle θ corresponds to 2 mrad. For Q_t = 0.12 MeV/c (interval 0-0.25 MeV/c) the corresponding opening angle is 0.05 mrad. In this Q_t interval there is a significant number of the simulated events with smaller Q_t, larger total momenta in the l.s. and opening angles smaller than 0.05 mrad. The contribution of these pairs to the total number of the simulated events in the Q_t interval allows checking the detection efficiency for the pairs with the opening angles of about 0.01 mrad.

The distribution with large Q_t allows checking and correcting the simulation procedure for the pairs with large opening angles in the l.s. The detection efficiency for these pairs is the product of the well-known efficiencies of the single particle detection. After the tuning of the simulation procedure and the evaluation of $|M_{\rm prod}|^2$ using these pair distributions, the expected numbers of the simulated Coulomb pairs in the intervals with small Q_t can be calculated with the theoretical accuracy better than 2%. The comparison of the numbers of the simulated pairs $NC_{\rm calc}$ and the numbers of the experimental pairs $NC_{\rm exp}$ allows checking and correcting the detection efficiency for the pairs with the small distance D.

References

[1] L. Afanasyev et al., Phys. Lett. B 255(1991)146.

[2] L. Nemenov, Yad. Fiz. 41 (1985) 980; Sov. J. Nucl. Phys. 41 (1985) 629.

[3] G. Gamov, Z. Phys. 51 (1928) 204.

[4] A. Sommerfeld, Atombau und Spektrallinien, F. Vieweg & Sohn (1931).

[5] A. D. Sakharov, Zh. Exp. Theor. Fiz. 18 (1948) 631,

[6] A.D. Sakharov, Sov. Phys. Usp. 34 (1991) 375.

[7] L. R. Wiencke, M. D. Church, E. E. Gottschalk, et al., Phys. Rev. D 46, 3708 (1992)

[8] L. Afanasyev et al., Phys. Lett. B 308 (1993) 200.

[9] B. Adeva et al., Phys. Lett. B 619 (2005) 50.

[10] B. Adeva et al., Phys. Lett. B 704 (2011) 24.

[11] R. Lednicky, J. Phys. G: Nucl. Part. Phys. 35 (2008) 125109.

[12] P.V.Chliapnikov, V.M.Ronjin, J.Phys.G: Nucl. Part. Phys. 36 (2009) 105004.
[13] M.V.Zhabitsky, DIRAC notes 2007-01, 2007-11, http://cdsweb.cern.ch/record/ 1369660
[14] M.V.Zhabitsky, Phys. At. Nucl. 71 (2008) 1040
[15] B. Adeva et al., Nucl. Instr. Meth. A 839 (2016) 52
[16] B. Adeva et al., Phys. Rev. D96 (2017) 052002.
[17] A. Benelli and V. Yazkov, Report No. DN-2016-01, http://cds.cern.ch/record/2137645
[18] O. Gorchakov and A. Kuptsov, DN (DIRAC Note) 2005-05; cds.cern.ch/record/1369686.
[19] O. Gorchakov, DN 2005-23; cds.cern.ch/record/1369668.
[20] M. Pentia et al., Nucl. Instr. Meth. A 795 (2015) 200.
[21] DIRAC Collaboration, dirac.web.cern.ch/DIRAC/offlinedocs/Userguide.html.
[22] A. Benelli, J. Smolik V. Yazkov, DN 2020-01; cds.cern.ch/record/2772989.
[23] P. Doskarova and V. Yazkov, DN 2013-05; cds.cern.ch/record/1628541.